Stretchable and Semitransparent Conductive Hybrid Hydrogels for Flexible Supercapacitors

Guang-Ping Hao,[†] Felix Hippauf,[†] Martin Oschatz,[†] Florian M. Wisser,[†] Annika Leifert,[†] Winfried Nickel,[†] Nasser Mohamed-Noriega,[†] Zhikun Zheng,[‡] and Stefan Kaskel[†,*]

[†]Department of Inorganic Chemistry, Dresden University of Technology, Bergstraße 66, Dresden 01069, Germany and [‡]Department of Materials, Swiss Federal Institute of Technology, ETH Zürich, Zürich 8093, Switzerland

ABSTRACT Conductive polymers showing stretchable and transparent properties have received extensive attention due to their enormous potential in flexible electronic devices. Here, we demonstrate a facile and smart strategy for the preparation of structurally stretchable, electrically conductive, and optically semitransparent polyaniline-containing hybrid hydrogel networks as electrode, which show high-performances in supercapacitor application. Remarkably, the stability can extend up to 35 000 cycles at a high current density of 8 A/g, because of the combined structural advantages in terms of flexible polymer chains, highly interconnected pores, and excellent contact between the host and guest functional polymer phase.

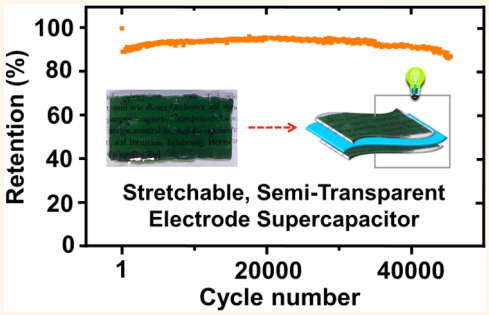

KEYWORDS: stretchable and transparent hydrogel · flexible supercapacitor · conductive polymer · long cycling stability · polyaniline

Stretchable, transparent, and electrically conductive materials are highly desired for next-generation flexible and transparent energy storage devices, electronics or sensors, which can go beyond to be applied in movable devices and arbitrary curved substrates.[1−6] To achieve this goal, the key issue is the simultaneous incorporation of mechanical robustness, optical transmittance and electronic conductivity. Conducting polymer hydrogels show great potential for the expected integration due to their excellent solid−liquid interface, good electric characteristics, and ease of processability.[7,8] So far, many aspects such as conductivity and morphology of conductive polymer hydrogels have been extensively studied.[9−11] However, the combination of stretchability and transparency is unique, and particularly long cycle stability has not been achieved before.[12−14]

Pan *et al.* have recently prepared a unique conductive hydrogel structure (polyaniline, PAni) *via* a direct polymerization of aniline (Ani) monomer in the presence of phytic acid (as both the gelator and dopant) and ammonium persulfate (as initiator).[10] The PAni hydrogel nanostructures showed excellent electronic conductivity and electrochemical properties, but the mechanical and optical properties were not investigated. Important advances have also been made toward flexibility and stretchability of hydrogels through combining two types of cross-linked polymers: ionically cross-linked alginate, and covalently cross-linked polyacrylamide.[15] However, the conductivity and transparency remained to be integrated. Very recently, Spinks and co-workers have succeeded in preparing an electrically conductive and mechanically robust hydrogel on the basis of poly(ethylene glycol) methyl ether methacrylate and poly(acrylic acid) (as host phase) and poly(3,4-ethylenedioxythiophene) (as electron conductive phase).[16] As the color of the materials was fully black (opaque), they did not show optical transmittance, and the long synthesis period of more than 2 weeks displayed an additional disadvantage.

Thus, a facile and rapid synthesis strategy for hydrogel networks with a high conductivity, stretchability and transparency remains to be addressed. One strategy to achieve such a multifunctional goal is to get a well designed preorganized host

* Address correspondence to Stefan.kaskel@chemie.tu-dresden.de.

Received for review April 14, 2014 and accepted June 29, 2014.

Published online June 30, 2014
10.1021/nn502065u

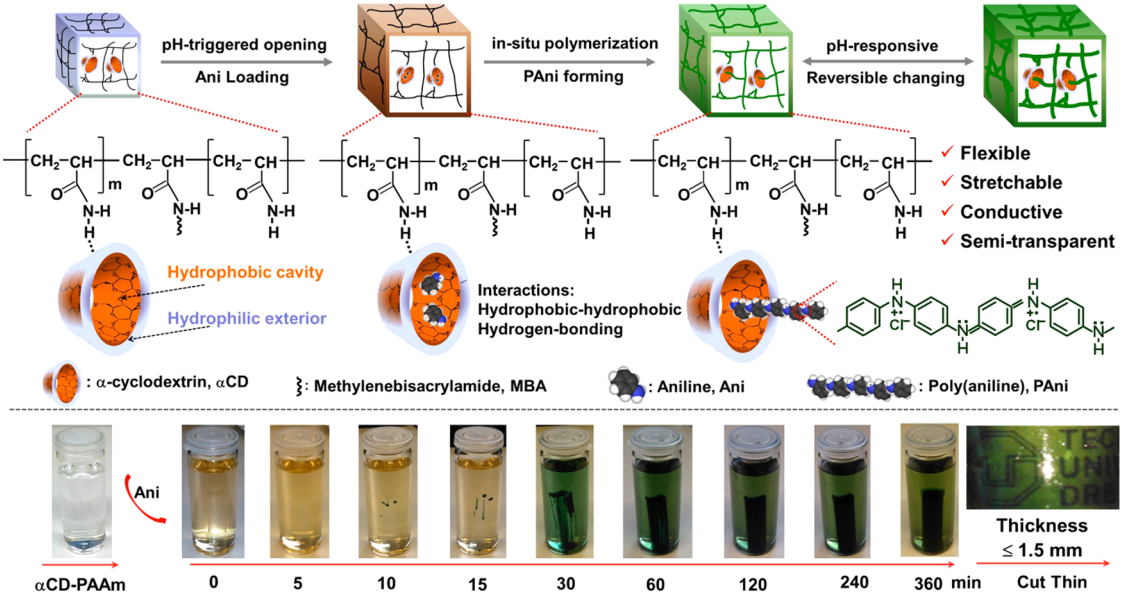

Figure 1. Synthesis principle (top) and rapid formation (bottom) of the structurally flexible and stretchable as well as electrically conductive hybrid hydrogel networks. The synthesis is based on preorganized αCD-containing polyacrylamide hydrogels that are amphiphilic and pH responsive. The conductive polymer networks become semitransparent for films with thickness ≤1.5 mm (bottom right shows the transparency on a curved surface).

phase with expected mechanical merits, interconnected pore systems as well as high affinity to the electron conductive phase. Generally, PAni as widely used and mature system is one of the most promising candidates as an electron conductive phase.[17,18] However, the hydrophobic properties of aniline monomers make them difficult to be compatible with highly hydrophilic host phase.[9,19] However, cyclodextrins (a family of cyclic carbohydrate compounds, *i.e.*, α-, *β*-, and *γ*-cyclodextrin (CD)) structurally show smart amphiphilic configuration,[20,21] which contains a hydrophobic cavity and hydrophilic exterior, resembling a "micro heterogeneous environment". Expectedly, hydrophobic compounds (in this case the Ani monomer) can easily accumulate in the hydrophobic cavity due to hydrophobic–hydrophobic interactions. Furthermore, the introduction of supramolecular cyclodextrin can improve their mechanical properties. For instance, Harada *et al.* reported well preorganized α/*β*-CD-containing hydrogels that showed significantly robust mechanical properties, even with self-healing capability.[22,23]

Combining the above considerations, we present a facile and rapid strategy to prepare highly flexible PAni-containing conductive hydrogel networks on the basis of preorganized α-CD-containing polyacrylamide (αCD-PAAm) hydrogels, showing highly homogeneous and interconnected macropores. Very interestingly, the obtained hybrid hydrogels show a perfect integration between the host phase (αCD-PAAm) and the PAni phase, in which the electroactive PAni can be well protected, ensuring a remarkable stability. Furthermore, semitransparent properties could be achieved even for film thickness up to 1.5 mm. On the basis of the multifunctional hybrid hydrogels, a prototypical foldable and stretchable supercapacitor is demonstrated, showing a remarkable stability up to 35 000 cycles at a high current density of 8 A/g.

RESULTS AND DISCUSSION

Figure 1 (top) depicts the preparation principle. The host αCD-PAAm hydrogel was prepared through a one-pot sol–gel process. The preorganized networks are pH responsive, highly porous and contain molecular level dispersed amphiphilic domains due to the participation of α-CD. Both of these characteristics greatly accelerate the loading of Ani monomers. The pH responsive properties ensure a swelling behavior, providing an open path for free diffusion of guest Ani molecules; while the amphiphilic properties ensure a hydrophobic–hydrophobic interaction, allowing an easy gathering of Ani molecules in the nonpolar cavities of α-CD. After Ani loading, the *in situ* polymerization can be triggered directly by immersing the swollen hydrogel into 1 M hydrochloric acid, without the need of an additional step for introducing the initiator ammonium persulfate (APS), because the APS is dispersed on molecular level in the preorganized αCD-PAAm in advance. This is much different to previous works that required an additional step to introduce the initiator,[9,16] again indicating the efficiency of our strategy.

When contacting the host αCD-PAAm (in the open state), the Ani monomers can freely diffuse into the whole αCD-PAAm networks, with the color change from transparent to light yellow, and subsequently to dark green (Figure 1 bottom and Figure 2a), indicating the *in situ* formation of PAni. The as-made αCD-PAAm-PAni network is highly stretchable and flexible

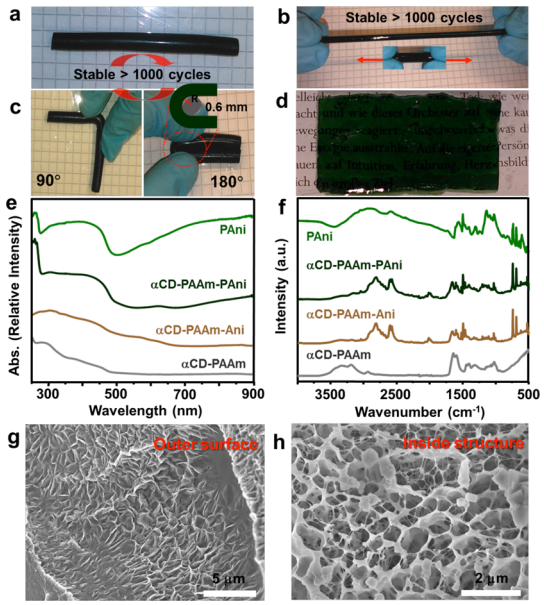

Figure 2. Structure characterization of αCD-PAAm-PAni: (a) as-made sample; (b and c) reversible deformation; (d) transparency illustration for film sample (thickness = 1.5 mm); (e and f) UV−vis and FT-IR spectra of dried samples in different processes; (g and h) SEM image detected for the outer surface and inside structure of the dried αCD-PAAm-PAni.

(Figure 2b), and can withstand deformation from arbitrary direction (Figure 2c). For example, the dark green hydrogel (original length, 25 mm; diameter, 5 mm) exhibited a significantly high stretchability (~4−5 times of its original length). We measured the length of the sample before and after stretching (Figure S1a,b) and estimated a stretching ratio of 5.1, which is a clear improvement for conductive hydrogels. Furthermore, the dark green rods (length, 68 mm; diameter, 5 mm) can be reversibly folded by 90° and 180°. The bending radius is measured to be as low as *ca.* 0.6 mm. There remain no visible changes like cracks or notches after stretching or folding it for more than 1000 cycles, indicating the robust mechanical properties of the αCD-PAAm-PAni hybrid network. Furthermore, the sample showed more flexible properties with the bending radius of *ca.* 0.4 mm when the sample is under a higher swelling ratio, which can even be in a spiral form itself around a stick with diameter of 0.8 mm (Figure S1c,d,e). More interesting, when the sample is cut thin or formed as film with thicknesses ≤1.5 mm, they become semitransparent, with dark green color throughout the whole structure (Figure 1 bottom right and Figure 2d).

Optical transmittance (Figure S2) of the αCD-PAAm-PAni hydrogel film (with thickness of 700 μm) over a wavelength range from 300 to 900 nm was measured with a UV−vis spectrometer using a blank glass substrate as the reference. The transmittance over visible light range (400−700 nm) first decreases from 59.5% (at 400 nm) to 20.1% (at 500 nm) and then recovers gradually reaching 98.2% at 837 nm in infrared radiation (700−900 nm) range. The electron conductivity of αCD-PAAm-PAni is estimated to be 0.39 S/cm, which outperforms most of PAni incorporated hybrid hydrogels, for example poly(acrylic acid),[24] chitosan,[25] *etc.*, even comparable to the pure PAni hydrogel.[10] We also observed that the resistivity only slightly changes during arbitrary shape deformation, which could enable a stable performance of flexible devices.

UV−vis and FT-IR spectroscopy were employed to analyze the chemical nature of the αCD-PAAm-PAni network. The broad band ranging from 310 to 480 nm (Figure 2e) is assigned to polaron to π^* band transition, while the long tail at wavelengths higher than 800 nm can be attributed to π to polaron band transition.[10,26] The UV−vis absorption patterns fit the features of the doped emeraldine state of PAni and are consistent with previously reported results.[27−29] The imine nitrogen protonated by the hydrochloric acid helps to delocalize the otherwise trapped diiminoquinone-diaminobenzene state, which allows a rapid electron transport, and thus, a good conductivity.[7,10] As compared to pure PAni, the free tail band of the αCD-PAAm-PAni network is weaker due to the hybridization of polymer chains. Moreover, the host phase (αCD-PAAm) and the host phase with the Ani monomer (αCD-PAAm-Ani) did not show free tail band (>800 nm), indicating the success of doping PAni to its conductive emeraldine state. FT-IR spectra (Figure 2f) of the αCD-PAAm-PAni showed the combined characteristic bands of both host structure and the active PAni phase, again confirming its hybrid nature. For example, the peaks at ~3352, ~3180, ~1660, and ~1605 cm^{-1} are attributed to the asymmetric and symmetric stretching of NH_2 and the Amide I and Amide II vibration (from PAAm);[30] the peaks at ~2943 and ~1075 cm^{-1} are attributed to the stretching of C−H and the bending vibration of O−H (from αCD);[31] the two strong peaks at ~2814 and 2589 cm^{-1} are attributed to stretching of N−H from the protonated (P)Ani; the peak at ~2000 cm^{-1} may relate to the absorption of free charge-carriers of the protonated PAni; the sharp peaks at ~1492 and 1451 cm^{-1} and in the region 764−665 cm^{-1} are attributed to the benzenoid ring stretching, the C═C stretching deformation of the quinoid ring, and the N−H wagging observed for primary and secondary amines (from PAni), respectively.[32]

The SEM images of the dried αCD-PAAm-PAni hybrid network reveal a uniform wrinkled surface texture (Figure 2g) with a repeat distance of 200−300 nm and interconnected pores throughout the whole inner structure (Figure 2h). The thickness of the surface wrinkles is less than 200 nm. When compared with the host structure (αCD-PAAm, Figure S3), the polymer chains of αCD-PAAm-PAni are thicker and the pores in between are more irregular, indicating the PAni filling into the pores of the host structure. Due to the highly homogeneous and interconnected pore system of the

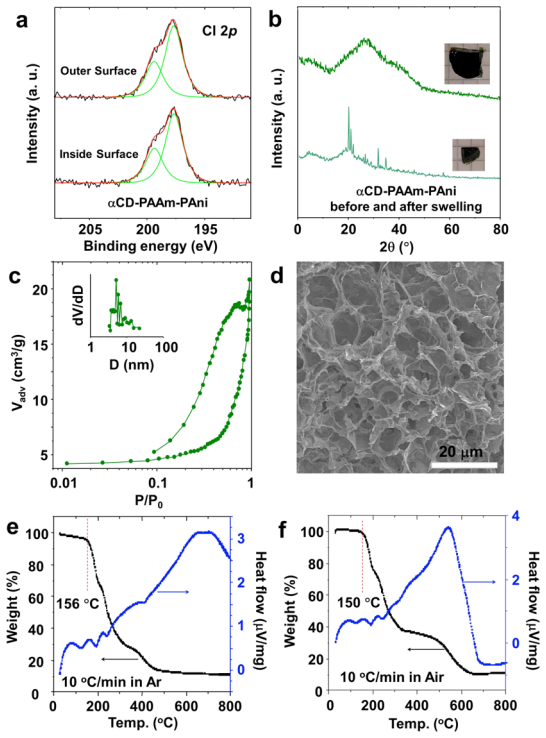

Figure 3. (a) XPS Cl 2p spectra, tested samples were taken from outer and inner part (5 mm below the surface) of a dried αCD-PAAm-PAni. (b) Powder XRD pattern of αCD-PAAm-PAni before and after swelling. (c) N_2 sorption isotherm, (d) SEM image, (e and f) simultaneous TG-DTA curve (in both Ar and air) of freeze-dried αCD-PAAm-PAni. The inset in (c) is the pore size distribution based on the BJH theory.

host structure, the loading of PAni was successful. Importantly, from the backbone of the polymer networks, one can not observe a phase transition between the host αCD-PAAm phase and the electronic conductive PAni phase, indicating a perfect integration of the hybrid polymer chains. This configuration is distinct from the most reported surface-grafting PAni over the substrate, which degraded rapidly during long-time cycling.[33,34] In this configuration, the αCD-PAAm not only acted as a host structure (loading the PAni) but also as a space buffer that could greatly mitigate the possible volume change (swelling and shrinking) of PAni during electrochemical process. The TG-DTA curves in Ar and air (Figure 3e,f) reflected the thermal stability of our hybrid samples. As can be seen, the hybrid polymers starts to decompose at a temperature around 150 °C both in Ar and in air, indicating the polymer backbones are stable under condition below 150 °C.

To analyze the composition and protonation condition, as well as the PAni dispersion in the αCD-PAAm-PAni, we recorded the XPS spectra (Figure 3a and XPS survey in Figure S4a,b), energy-dispersive X-ray spectroscopy (EDS in Figure S5), and elemental analysis (Table S1). Both the XPS and the EDS data confirmed the existence of elements of C, O, N, and Cl, with the atomic content of around 71%, 11%, 18%, and 1%, respectively. The elemental analysis also confirmed the elements of C, N, and H, with a C/N ratio of 4.25:1, which is close to that of XPS and EDS results. From Figure 3a, the Cl 2p spectra with the peak at 199.4 and 197.7 eV revealed the existence of Cl $2p_{1/2}$ and Cl $2p_{3/2}$, respectively, which corresponds to the Cl in the ionic state. The XPS results confirm the good protonation of PAni even in the inside structure, indicating a good dispersion of PAni throughout the sample. Such protonation characteristics are consistent with previous reports by Yue and Epstein.[35] By comparing the XRD pattern of the αCD-PAAm-PAni (Figure 3b) with that of the host structure (αCD-PAAm) and the PAni (Figure S6), we could further confirm the hybrid nature of αCD-PAAm-PAni. Taking together the SEM observations, XPS spectra, and the XRD patterns, we could conclude the PAni is stably embedded in the hybrid structure.

The transport of ions and small molecules in between PAni sites could be substantially accelerated for samples in the swollen state due to the pore channel opening. This may lead to a high electrochemical performance. The intensity of the peaks (Figure 3b) in the range of $2\theta = 20.0-40.0°$ were significantly decreased, implying the loss of structure ordering during swelling, and the increase of distance of polymer chains. In contrast, the peak at $2\theta = 20.1°$ for the dried sample shifted to $2\theta = 28.0°$ for the swollen sample, indicating that the distance of $\pi-\pi$ stacking (periodicity perpendicular to the polymer chains) obviously decreased, potentially increasing the conductivity of the αCD-PAAm-PAni.

To elucidate the porous structures of αCD-PAAm-PAni in the swollen state, we conducted the fast freeze-drying, and then tested the N_2 physisorption (Figure 3c) and performed SEM observations of the freeze-dried sample (Figure 3d). N_2 physisorption results showed a type III isotherm, with a BET surface area of 16 $m^2\ g^{-1}$. The clear hysteresis loop revealed the existence of mesopores. The large nitrogen uptake at a high relative pressure of P/P_0 of 0.9−1 indicates the characteristic macroporosity. Furthermore, the SEM images showed a sponge-like morphology with highly interconnected pore channels, which is consistent with the N_2 sorption results. The pore voids of the freeze-dried sample are derived from the replica of ice crystals. Thus, in the swollen state of αCD-PAAm-PAni in supercapacitor tests, one could imagine that the macropores and mesopores are fully filled with electrolytes, significantly accelerating the diffusion of electrolyte ions.

As demonstrated above, our αCD-PAAm-PAni hybrid hydrogel networks exhibit highly foldable and stretchable capability, good optical transmittance as well as good conductivity. These merits enable a great potential for next-generation supercapacitors. Furthermore, previous results showed that hydrogels as electrode could generate an excellent interface between the electron transport phase (electrode) and the ion

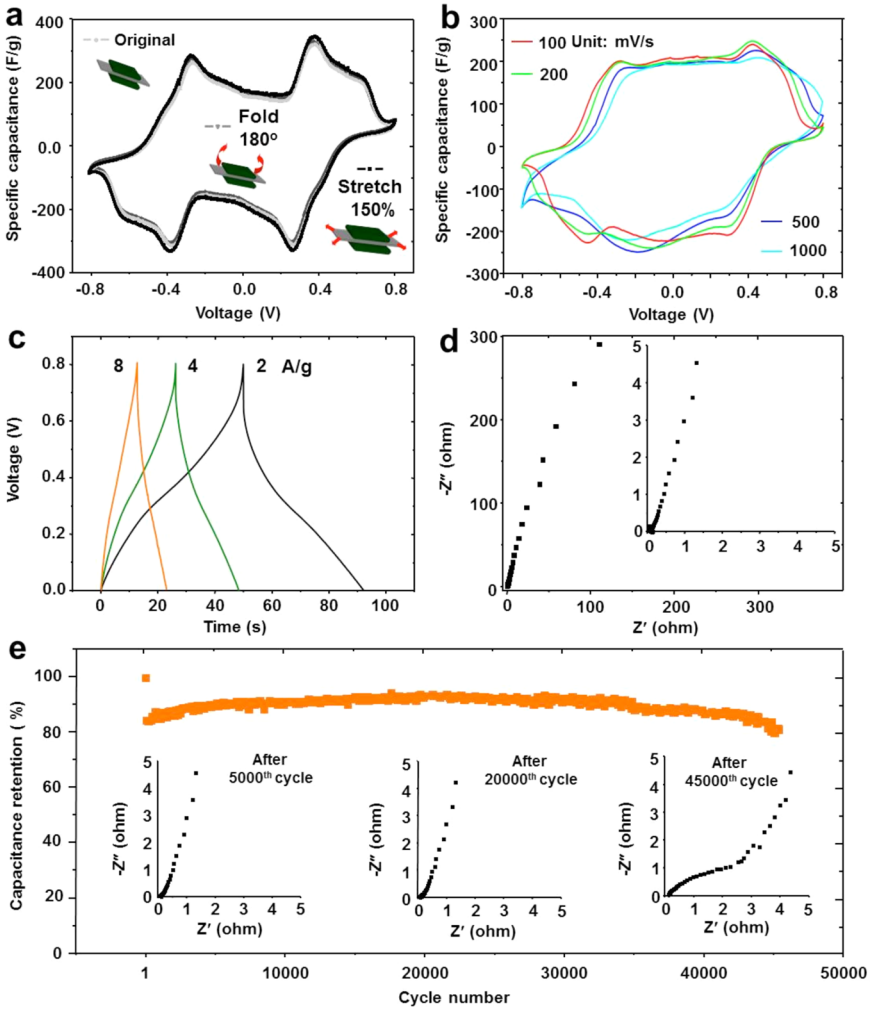

Figure 4. Foldable and stretchable supercapacitors tests under room temperature with 1 M H_2SO_4 as electrolyte. (a) Cyclic voltammogram curves of the flexible conductive hydrogel electrode-based supercapcitors with different geometries at a scan rate of 10 mV/s. (b) Cyclic voltammogram curves at different scan rates of 100−1000 mV/s. (c) Galvanostatic charge−discharge profiles at various current densities. (d) Impedance curve of the stretched supercapacitor electrode. (e) Galvanostatic charge−discharge cycling test at a current density of 8 A/g; inset shows the impedance curve tracked during the long cycles.

transport phase (electrolyte), and thus, the charge and mass diffusion resistance can be greatly reduced.[10,36] Interestingly, the electrolyte permeation of the αCD-PAAm-PAni can be well controlled according to its pH-responsive property. Thus, before each test, the assembled supercapacitor was soaked in electrolyte to reach the wetted state. The highly interconnected pore channels will reduce the diffusion path for electrolyte ions to access the electroactive surface of PAni.

The electrochemical properties of our conductive hybrid polymer networks-based supercapacitors were tested in a two-electrode "sandwich" configuration. We first studied the cyclic voltammetry (CV) of αCD-PAAm-PAni with different geometries (original state, folded by 180° and linearly stretched by 150%) to analyze the capacitance behavior of PAni within a potential range of −0.8 to 0.8 V at a scan rate of 10 mV/s in 1 M H_2SO_4 electrolyte (Figure 4a). In each geometry, the redox peaks (due to the leucoemeraldine/emeraldine and emeraldine/pernigraniline transitions of PAni) in the CV curves came out at almost the same position, which indicates the stable pseudocapacitive behavior during shape deformation. Among them, the stretched electrode showed a slightly enhanced specific capacitance of 315 F/g on the basis of total active mass (dry weight) of PAni. This could be due to the larger contacting area as compared to other geometries. The electrode capacitance calculated for the original state and folded geometry are in the same level, *i.e.*, 304 and 301 F/g, respectively. Considering the mass ratio (*ca.* 13 wt %) of PAni in the hybrid polymer, the specific capacitance on the basis of the whole dry mass is 41 F/g for the stretched electrode. Furthermore, the rate-dependent CVs were recorded on the stretched sample at scan rates from 100 to 1000 mV/s (Figure 4b). A linear dependence between discharge current and scan rate is found to be up to 1000 mV/s in the capacitive region, indicating a high power capability for the supercapacitor

based on αCD-PAAm-PAni. This scan rate is 5 to 10 times higher than previously results reported with PAni hydrogels,[10] PAni-polymer (*e.g.*, chitosan, cellulose, *etc.*) composites,[25,37] and even PAni-carbon (*e.g.*, graphene, CNT, nanodiamond) composites.[38−40] At high scan rate (1000 mV/s), the deviation of CV curves was observed because the redox reactions could not proceed completely over the inner active sites in such short time. This phenomenon was also observed in reported results at lower scan rates of 100−200 mV/s.[25−40] The specific capacitances at scan rates of 100, 200, 500, and 1000 mV/s are 290, 290, 265, and 242 F/g, respectively, with the calculated capacitance retention of 92%, 92%, 84%, and 77% accordingly, indicating a good rate performance of the αCD-PAAm-PAni electrode.

Galvanostatic charge−discharge (CD) measurements were performed at current densities of 2, 4, and 8 A/g (Figure 4c). The corresponding specific capacitances derived from discharge curves are ∼322, 308, and 282 F/g, respectively. This revealed the αCD-PAAm-PAni based electrodes could retain 96% and 88% capacitance when current density was increased by a factor of 2 and 4, again indicating the good rate performance. The impedance curve of the assembled supercapacitor was tested (Figure 4d) to evaluate the electronic and ionic transport of αCD-PAAm-PAni electrode in electrolyte. The nearly vertical shape at lower frequencies indicates an ideal capacitive behavior of the electrodes. From the magnified high-frequency regions in the inset of Figure 4d, the equivalent series resistance (ESR) is estimated to be ∼0.2 Ω, which indicates the small overall resistance from active material, the contact resistance at the electrode−electrolyte interface and the solution resistance. The nonvisible semicircle also indicates the very low ion transport resistance within the pores of αCD-PAAm-PAni polymer networks. Similar phenomenon was also observed for the pure PAni hydrogels.[10]

Interestingly, the αCD-PAAm-PAni-based supercapacitors deliver a remarkable cycling stability up to 35 000 cycles, which is an important advance in conductive polymer electrode. Generally, the capacitance of the previously reported PAni-based supercapacitors decreased by 40−50% over 1000 cycles,[33,41] because of the possible swelling and shrinking of the active PAni during charging and discharging.[42] The perfectly integrated hybrid structure of the αCD-PAAm-PAni electrode as well as the flexible nature of the polymer networks may greatly buffer the volume changes during the intensive cycling processes, and thus a high capacitance retention up to 92% can be obtained after 35 000 cycles, and 80% after 45 000 cycles at a high current density of 8 A/g. To understand the changes of electronic and ionic transport during such long cycles, we tested the impedance curve after the 5000th cycle, 20 000th cycle, and 45 000th cycle, respectively (Figure 4e inset). After 5000 and 20 000 cycles, the vertical shape of the impedance curve at lower frequencies and the low ESR (<0.2 Ω) was retained, confirming the structure robustness of the αCD-PAAm-PAni hydrogels, while after 45 000 cycles, the impedance curve changed greatly. A big semicircle started to come out, indicating the increasing resistance for ions transport within the αCD-PAAm-PAni polymer networks.

To analyze possible mechanism (the stability and degradation), we tested and compared the FT-IR spectra (Figure 5a) of the as-prepared sample with that of after 50 000 cycling (at this stage the supercapacitor performance degraded clearly). As can be seen, after so long cycles, the characteristic bands for active PAni significantly changed, while several new bands (*e.g.*, 600 and 900 cm^{-1}) related to sulfonic groups from the adsorbed sulfuric acid appeared. This reveals that the degradation of αCD-PAAm-PAni-based supercapacitor is mostly due to the leaching of active PAni species. For example, the missing bands include the stretching of N−H from protonated (P)Ani with peaks at ∼2814 and 2589 cm^{-1}; the absorption of free charge-carriers of the protonated PAni with the peak at ∼2000 cm^{-1}; and the N−H wagging for primary and secondary amines (from PAni) with peaks in the region 764−665 cm^{-1}. This, on the other hand, indicates that the cycling stability of the αCD-PAAm-PAni system is due to the protecting effect of the host polymer matrix that against the leaching of active PAni in our system. Because of this, the hybrid PAni samples can outperform other surface coated PAni or PAni based materials.[33,41]

We also tried to increase the overall capacitance of the αCD-PAAm-PAni electrode by increasing the PAni content in the hybrid hydrogel, which can be achieved by extending the loading time of Ani from 6 to 72 h. The formation of PAni in the first 6 h was most rapid, then increased gradually to *ca.* 25 wt % of PAni after 48 h, and further to *ca.* 28 wt % PAni in the dry hybrid polymer after 72 h, showing much darker green color. The loading rate decreased probably because the first polymerized PAni occupied a large part of open macropores and mesopores, which consequently reduce their loading rate. From the CV curves and CD profiles for sample with 28 wt % PAni content (Figure 5b,c), the capacitive properties of PAni were almost remained as compared to sample with low PAni content above. We calculated the specific capacitances to be ∼311, 298, and 279 F/g at 2, 4, and 8 A/g on the basis of the active PAni (Figure 5c). Following these analysis, the overall capacitance of electrode with 25 and 28 wt % PAni loading were calculated to be 73 and 81 F/g on the whole dry mass of the electrode. Considering the high water content, the overall capacitance on the basis of the whole hydrogel still remains to be increased toward actual supercapacitor application.

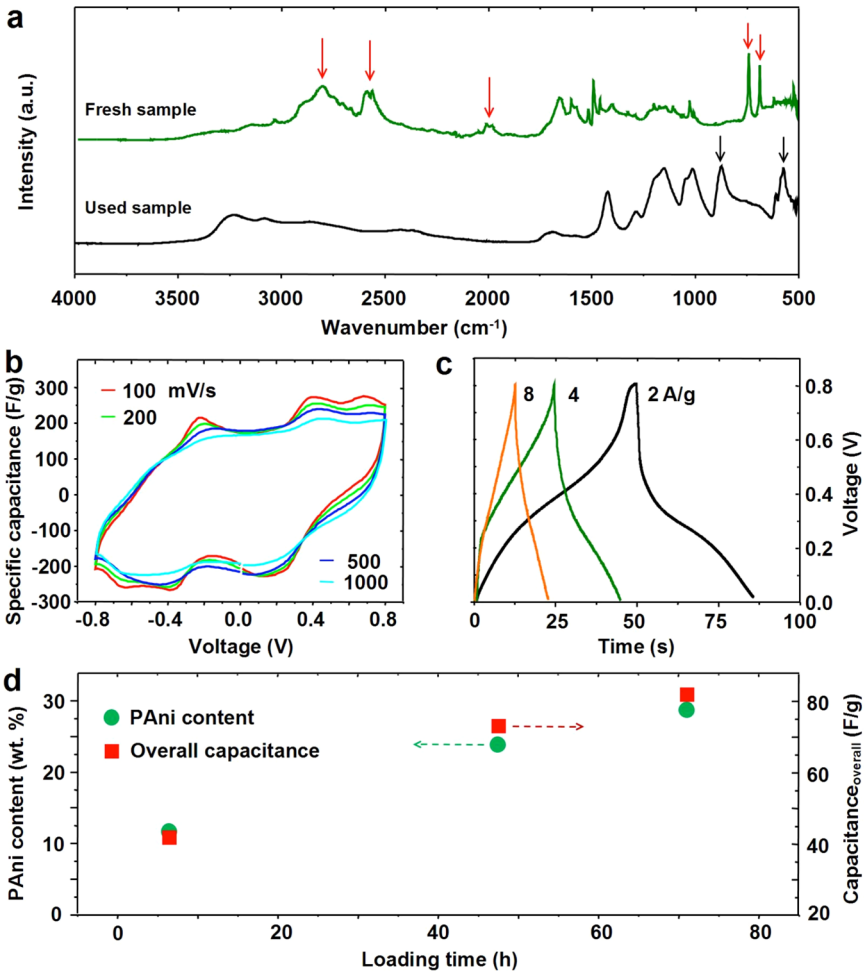

Figure 5. (a) FT-IR spectra of the as-prepared samples and the sample after 50 000 cycles test. Before FT-IR test, the samples are fully dried at 80 °C for 24 h. (b) Cyclic voltammogram curves at different scan rates of 100−1000 mV/s of samples with PAni loading of 28 wt % in the dry hybrid polymer. (c) Galvanostatic charge−discharge profiles at various current densities of samples with PAni loading of 28 wt % in the dry hybrid polymer. (d) The relationship among the loading time, the PAni content in the dry hybrid polymer, and the overall electrode capacitance on the basis of the whole dry mass of the electrode.

Besides the above characteristics, the synthesis strategy offers a high flexibility in product form control and processing scalability. Samples in the form of monoliths, films, rods *etc.* could be prepared depending on the container, exhibiting great convenience for their application. For example, in the above supercapacitor test, the αCD-PAAm-PAni film was directly employed as formed, without the need of any binders.

CONCLUSION

In summary, the synthesis based on the synergistic combination of the hydrophobic−hydrophobic interactions and the pH-triggered opening effect for hydrogel networks with a high conductivity, stretchability, and transparency has been demonstrated to be facile and rapid. On the basis of the high conductivity, mechanical flexibility, and stretchability, the αCD-PAAm-PAni hybrid networks showed great potential in application as flexible electrode, which showed an excellent rate performance and a remarkable cycling stability. We believe the synthesis strategy of the αCD-PAAm-PAni networks, as well as their high-performance in flexible supercapacitors, may have a major impact on the advance of new type conductive hydrogels materials for next-generation energy storage devices. The effort to improve the overall capacitance using this synthesis system is still ongoing; we hope the overall capacitance could also be in a leading position in the future.

METHODS

Fabrication of Materials. *Thermal Radical Polymerization for the Synthesis of αCD-PAAm Host Hydrogel.* In a typical synthesis, αCD and AAm monomer with weight ratio of αCD/AAm of 1:4 were dissolved in deionized (DI) water. Then, the cross-linking agent (*N*,*N*′-methylenebis(acrylamide), MBA) and thermo-initiator (ammonium persulfate) of weight ratio 0.05% and 4.69%, respectively, relative to AAm monomer, were added into the solution. When completely dissolved at 25 °C, the solution was transferred into glass molds with desired size, and then

the mold was placed in an oven at 50 °C until solidification, to form finally the αCD-PAAm host hydrogel.

Synthesis of αCD-PAAm-PAni Hybrid Hydrogel. After quickly rinsing with DI water, a certain amount of αCD-PAAm (*e.g.*, 1.0 g) was immersed in the Ani/HCl solution prepared by mixing Ani solution (1 mL of Ani in 30 mL of DI water) and 10 mL of HCl solution (1 M) at ambient temperature for a desired time for the swelling and loading of Ani as well as their *in situ* polymerization into PAni, ending with dark green αCD-PAAm-PAni hybrid hydrogel. To tune the mass loading of PAni, the immersion time of host hydrogel in the Ani/HCl solution was changed from 6 to 48 h and further to 72 h.

Structural and Properties Characterization. The UV−vis absorbance spectra were collected using a Varian spectrophotometer equipped with a praying mantis (Harrick Scientific Products). The FT-IR spectra were recorded on a BRUKER Vertex 70 Spectrometer with the help of a golden gate ATR-unit (32 scans, 4000−500 cm^{-1}, resolution 1 cm^{-1}). XPS spectra were acquired with a PHI Quantera SXM spectrometer (ULVAC-PHI, Chanhassen, MN) equipped with an Al Kα monochromatic source. All the spectra were calibrated using the C 1s neutral-carbon peak at 284.6 eV. Powder XRD patterns were collected on a STOE STADI P diffractometer operated at 40 kV and 30 mA with monochromated Cu Kα1 (λ = 0.15405 nm) radiation and with a scan speed of 30 s/step and a step size of 0.1°. The conductivity was measured with a linear probe head (Keithley 2400) using four-point probe technique. Scanning electron microscopy (SEM) was performed on a Zeiss DSM 982 Gemini instrument. Thermogravimetric analysis (TG-DTA) was carried out on a NETZSCH STA 409 PC/PG instrument at a heating rate of 10 °C min^{-1} under both argon and air atmosphere. Elemental analysis was recorded on a EuroEA Elemental Analyzer.

Electrochemical Tests. Prototype supercapacitor was assembled in a symmetrical two-electrode using a similar procedure reported by Li *et al.*[36] Before each test, the electrode was soaked in electrolyte to reach the fully wetted state. To assemble the supercapacitor, two pieces of hydrogels with the same size (∼8 mm × ∼8 mm, thickness of ∼700 μm, areal mass loading of PAni: *ca.* 3.4, 6.4, and 7.2 mg/cm^2) were first attached on two Pt foils, which were separated by glass fiber separator MN 85/70 with organic binder from Macherey-Nagel. After it was wrapped with parafilm, the prototype supercapacitor was immersed in 1 M H_2SO_4 solution as the electrolyte. All the electrochemical measurements were carried out using Ivium-Sate electrochemical interface and impedance analyzer. The cyclic voltammetry (CV) was performed in the range of −0.8 to 0.8 V, electrochemical impedance spectroscopy (EIS) in the frequency range of 1 mHz to 100 kHz with a 10 mV AC amplitude, and galvanostatic charge−discharge test in the range of 0 to 0.8 V at the current density of 2, 4, and 8 A/g. All electrochemical tests were carried out at room temperature (22 °C). The calculation of specific gravimetric capacitance of the supercapacitor cell based on CV and galvanostatic charge−discharge data was referred to the reported works[40,43] by Yushin *et al.*

Conflict of Interest: The authors declare no competing financial interest.

Supporting Information Available: Figures S1−S6 and Table S1 for preliminary mechanical test, optical transmittance test result, SEM images, XPS survey spectra, EDS data, the XRD patterns, and elemental analysis (details as described in the text), respectively. This material is available free of charge *via* the Internet at http://pubs.acs.org.

Acknowledgment. This work was financially supported by the DFG and Alexander von Humboldt Foundation. We thank C. Fischer and E. Brunner (Institute for Bioanalytical Chemistry, Technical University Dresden) for freeze-drying, J. Deng for helpful discussion regarding SEM measurement, and S. Zschoche and K. Schneider (Leibniz Institute of Polymer Research Dresden) for helpful mechanical test.

REFERENCES AND NOTES

1. Pang, C.; Lee, G.-Y.; Kim, T.; Kim, S. M.; Kim, H. N.; Ahn, S.-H.; Suh, K.-Y. A Flexible And Highly Sensitive Strain-Gauge Sensor Using Reversible Interlocking of Nanofibres. *Nat. Mater.* **2012**, *11*, 795–801.
2. Keplinger, C.; Sun, J.-Y.; Foo, C. C.; Rothemund, P.; Whitesides, G. M.; Suo, Z. Stretchable, Transparent, Ionic Conductors. *Science* **2013**, *341*, 984–987.
3. Lu, A.-H.; Hao, G.-P.; Sun, Q. Design of Three-Dimensional Porous Carbon Materials: From Static to Dynamic Skeletons. *Angew. Chem., Int. Ed.* **2013**, *52*, 7930–7932.
4. Presser, V.; Zhang, L.; Niu, J. J.; McDonough, J.; Perez, C.; Fong, H.; Gogotsi, Y. Flexible Nano-Felts of Carbide-Derived Carbon with Ultra-High Power Handling Capability. *Adv. Energy Mater.* **2011**, *1*, 423–430.
5. Meng, Y.; Wang, K.; Zhang, Y.; Wei, Z. Hierarchical Porous Graphene/Polyaniline Composite Film with Superior Rate Performance for Flexible Supercapacitors. *Adv. Mater.* **2013**, *25*, 6985–6990.
6. Wang, K.; Wu, H.; Meng, Y.; Zhang, Y.; Wei, Z. Integrated Energy Storage And Electrochromic Function in One Flexible Device: An Energy Storage Smart Window. *Energy Environ. Sci.* **2012**, *5*, 8384–8389.
7. Snooka, G. A.; Kao, P.; Best, A. S. Conducting-Polymer-Based Supercapacitor Devices and Electrodes. *J. Power Sources* **2011**, *196*, 1–12.
8. Zhao, Y.; Liu, B.; Pan, L.; Yu, G. 3D Nanostructured Conductive Polymer Hydrogels for High-Performance Electrochemical Devices. *Energy Environ. Sci.* **2013**, *6*, 2856–2870.
9. Tang, Z.; Wu, J.; Liu, Q.; Zheng, M.; Tang, Q.; Lan, Z.; Lin, J. Preparation of Poly(acrylic acid)/Gelatin/Polyaniline Gel-Electrolyte and Its Application in Quasi-Solid-State Dye-Sensitized Solar Cells. *J. Power Sources* **2012**, *203*, 282–287.
10. Pan, L.; Yu, G.; Zhai, D.; Lee, H. R.; Zhao, W.; Liu, N.; Wang, H.; Tee, B. C.-K.; Shi, Y.; Cui, Y.; *et al.* Hierarchical Nanostructured Conducting Polymer Hydrogel with High Electrochemical Activity. *Proc. Natl. Acad. Sci. U.S.A.* **2012**, *109*, 9287–9292.
11. Wang, K.; Wu, H.; Meng, Y.; Wie, Z. Conducting Polymer Nanowire Arrays for High Performance Supercapacitors. *Small* **2014**, *10*, 14–31.
12. Rogers, J. A. A Clear Advance in Soft actuators. *Science* **2013**, *341*, 968–969.
13. Bauer, S. Flexible Electronics: Sophisticated Skin. *Nat. Mater.* **2013**, *12*, 871–872.
14. Palleau, E.; Reece, S.; Desai, S. C.; Smith, M. E.; Dickey, M. D. Self-Healing Stretchable Wires for Reconfigurable Circuit Wiring and 3D Microfluidics. *Adv. Mater.* **2013**, *25*, 1589–1592.
15. Sun, J.-Y.; Zhao, X.; Illeperuma, W. R. K.; Chaudhuri, O.; Oh, K. H.; Mooney, D. J.; Vlassak, J. J.; Suo, Z. Highly Stretchable and Tough Hydrogels. *Nature* **2012**, *489*, 133–136.
16. Naficy, S.; Razal, J. M.; Spinks, G. M.; Wallace, G. G.; Whitten, P. G. Electrically Conductive, Tough Hydrogels with pH Sensitivity. *Chem. Mater.* **2012**, *24*, 3425–3433.
17. Lu, W.; Fadeev, A. G.; Qi, B.; Smela, E.; Mattes, B. R.; Ding, J.; Spinks, G. M.; Mazurkiewicz, J.; Zhou, D.; Wallace, G. G.; *et al.* Use of Ionic Liquids for π-Conjugated Polymer Electrochemical Devices. *Science* **2002**, *297*, 983–987.
18. Benson, J.; Kovalenko, I.; Boukhalfa, S.; Lashmore, D.; Sanghadasa, M.; Yushin, G. Multifunctional CNT-polymer Composites for Ultra-Tough Structural Supercapacitors and Desalination Devices. *Adv. Mater.* **2013**, *25*, 6625–6632.
19. Wu, J. H.; Lan, Z.; Lin, J. M.; Huang, M. L.; Hao, S. C.; Sato, T.; Yin, S. A Novel Thermosetting Gel Electrolyte for Stable Quasi-solid-state Dye-sensitized Solar Cells. *Adv. Mater.* **2007**, *19*, 4006–4011.
20. Del Valle, E. M. M. Cyclodextrins and Their Uses: A Review. *Process Biochem.* **2004**, *39*, 1033–1046.
21. Peters, O.; Ritter, H. Supramolecular Controlled Water Uptake of Macroscopic Materials by A Cyclodextrin-Induced Hydrophobic-to-Hydrophilic Transition. *Angew. Chem., Int. Ed.* **2013**, *52*, 8961–8963.

22. Nakahata, M.; Takashima, Y.; Hashidzume, A.; Harada, A. Redox-Generated Mechanical Motion of A Supramolecular Polymeric Actuator Based on Host–Guest Interactions. *Angew. Chem., Int. Ed.* **2013**, *52*, 5731–5735.
23. Kakuta, T.; Takashima, Y.; Nakahata, M.; Otsubo, M.; Yamaguchi, H.; Harada, A. Preorganized Hydrogel: Self-Healing Properties of Supramolecular Hydrogels Formed by Polymerization of Host–Guest-Monomers that Contain Cyclodextrins and Hydrophobic Guest Groups. *Adv. Mater.* **2013**, *25*, 2849–2853.
24. Xia, Y.; Zhu, H. Polyaniline Nanofiber-Reinforced Conducting Hydrogel with Unique pH-Sensitivity. *Soft Matter* **2011**, *7*, 9388–9393.
25. Ismail, Y. A.; Chang, J.; Shin, S. R.; Mane, R. S.; Han, S.-H.; Kim, S. J. Hydrogel-Assisted Polyaniline Microfiber as Controllable Electrochemical Actuatable Supercapacitor. *J. Electrochem. Soc.* **2009**, *156*, A313–A317.
26. Chiou, N.-R.; Epstein, A. J. Polyaniline Nanofibers Prepared by Dilute Polymerization. *Adv. Mater.* **2005**, *17*, 1679–1683.
27. Huang, J.; Virji, S.; Weiller, B. H.; Kaner, R. B. Polyaniline Nanofibers: Facile Synthesis and Chemical Sensors. *J. Am. Chem. Soc.* **2003**, *125*, 314–315.
28. Li, W.; Wang, H.-L. Oligomer-Assisted Synthesis of Chiral Polyaniline Nanofibers. *J. Am. Chem. Soc.* **2004**, *126*, 2278–2279.
29. Zhang, X.; Goux, W. J.; Manohar, S. K. Synthesis of Polyaniline Nanofibers by "Nanofiber Seeding". *J. Am. Chem. Soc.* **2004**, *126*, 4502–4503.
30. Chiem, L. T.; Huynh, L.; Ralston, J.; Beattie, D. A. An *in Situ* ATR–FTIR Study of Polyacrylamide Adsorption at the Talc Surface. *J. Colloid Interface Sci.* **2006**, *297*, 54–61.
31. Sambasevam, K. P.; Mohamad, S.; Sarih, N. M.; Ismail, N. A. Synthesis and Characterization of the Inclusion Complex of β-Cyclodextrin and Azomethine. *Int. J. Mol. Sci.* **2013**, *14*, 3671–3682.
32. Trchová, M.; Stejskal, J. Polyaniline: The Infrared Spectroscopy of Conducting Polymer Nanotubes (IUPAC Technical Report). *Pure Appl. Chem.* **2011**, *83*, 1803–1817.
33. Cong, H.-P.; Ren, X.-C.; Wang, P.; Yu, S.-H. Flexible Graphene–Polyaniline Composite Paper for High-Performance Supercapacitor. *Energy Environ. Sci.* **2013**, *6*, 1185–1191.
34. Zhang, H.; Wang, J.; Chen, Y.; Wang, Z.; Wang, S. Long-Term Cycling Stability of Polyaniline on Graphite Electrodes Used for Supercapacitors. *Electrochim. Acta* **2013**, *105*, 69–74.
35. Yue, J.; Epstein, A. J. XPS Study of Self-Doped Conducting Polyaniline and Parent Systems. *Macromolecules* **1991**, *24*, 4441–4445.
36. Yang, X.; Zhu, J.; Qiu, L.; Li, D. Bioinspired Effective Prevention of Restacking in Multilayered Graphene Films: towards the Next Generation of High-Performance Supercapacitors. *Adv. Mater.* **2011**, *23*, 2833–2838.
37. Zhang, X.; Lin, Z.; Chen, B.; Zhang, W.; Sharma, S.; Gu, W.; Deng, Y. Solid-State Flexible polyaniline/silver Cellulose Nanofibrils Aerogel supercapacitors. *J. Power Sources* **2014**, *246*, 283–289.
38. Cheng, Q.; Tang, J.; Shinya, N.; Qin, L.-C. Polyaniline Modified Graphene and Carbon Nanotube Composite Electrode for Asymmetric Supercapacitors of High Energy Density. *J. Power Sources* **2013**, *241*, 423–428.
39. Xu, Y.; Schwab, M. G.; Strudwick, A. J.; Hennig, I.; Feng, X.; Wu, Z.; Müllen, K. Screen-Printable Thin Film Supercapacitor Device Utilizing Graphene/Polyaniline Inks. *Adv. Energy Mater.* **2013**, *3*, 1035–1040.
40. Kovalenko, I.; Bucknall, D. G.; Yushin, G. Detonation Nanodiamond and Onion-Like-Carbon-Embedded Polyaniline for Supercapacitors. *Adv. Funct. Mater.* **2010**, *20*, 3979–3986.
41. Sivakkumara, S. R.; Kima, W. J.; Choia, J.-A.; MacFarlaneb, D. R.; Forsythc, M.; Kim, D.-W. An Improved Dynamic Model Considering Effects of Temperature and Equivalent Internal Resistance for PEM Fuel Cell Power Modules. *J. Power Sources* **2007**, *171*, 1062–1068.
42. Rudge, A.; Davey, J.; Raistrick, I.; Gottesfeld, S.; Ferraris, J. P. Conducting Polymers as Active Materials in Electrochemical Capacitors. *J. Power Sources* **1994**, *47*, 89–107.
43. Korenblit, Y.; Rose, M.; Kockrick, E.; Borchardt, L.; Kvit, A.; Kaskel, S.; Yushin, G. High-Rate Electrochemical Capacitors Based on Ordered Mesoporous Silicon Carbide-Derived Carbon. *ACS Nano* **2010**, *4*, 1337–1344.